Modeling for Postyield Buckling of Reinforcement

Rajesh Prasad Dhakal[1] and Koichi Maekawa[2]

Abstract: Finite element microanalysis using fiber technique was carried out to study the buckling mechanism of reinforcing bars. It was found that reinforcing bars under inelastic axial compression exhibit lateral deformation defined as buckling due to the geometrical nonlinearity. Further investigation revealed that the postbuckling average compressive stress is less than the local stress corresponding to the same strain due primarily to the different stiffness for loading and unloading fibers in the laterally deformed section. It was clarified that the average compressive stress-strain relationship including the softening in the postbuckling range can be completely described in terms of the product of square root of yield strength and the slenderness ratio of the reinforcing bar. Moreover, a unique relationship between the average stress and average strain of reinforcing bars including the effect of buckling is established through various parametric analyses. The comparison of the analytical results and proposed model with some experimental results showed good agreement, thus verifying the reliability of the microanalysis and proposed computational model.

DOI: 10.1061/(ASCE)0733-9445(2002)128:9(1139)

CE Database keywords: Buckling; Deformation; Stress-strain relations; Reinforcement.

Introduction

In reinforced concrete members, the reinforcing bars might undergo high-compressive strain, which induces large lateral deformation of reinforcing bars, hereafter referred to as buckling. Because of geometrical nonlinearity, average compressive stress carried by reinforcing bar decreases in the postbuckling range. However, in tension, geometrical nonlinearity does not prevail as no lateral deformation is induced even after yielding. Consequently, the average tensile stress-strain relationship over the specified control volume is exactly the same as the point wise tensile stress-strain relationship. Therefore, using similar average stress-strain behavior for reinforcing bars in tension and compression seems unconvincing.

Of course, the point wise stress-strain behavior of reinforcing bars in compression is also the same as that in tension because the point wise relationships are not influenced by the change in geometry (Dodd and Restrepo-Posada 1995). Hence, using the point wise stress-strain relationship can account for the lateral deformation of compressed longitudinal reinforcing bars provided that the control volume, over which the average stress-strain relationship is computed, is very small. However, in the finite element structural analysis of larger scale, such small element size is not feasible because of the long computation time and large memory required. For finite element analysis of reinforced concrete structures with substantial element size, an average stress-strain relationship of reinforcing bars that takes into account the effect of buckling is needed. Hence, this research aims to formulate a versatile average stress-strain relationship that can be applied to reinforcing bars with any geometrical and mechanical properties.

To generate the data for model formulation, a parametric study based either on experiment or analysis is necessary. There are some experimental studies performed in the past to clarify the buckling mechanism of bare bar (Monti and Nuti 1992; Rodriguez et al. 1999). Tests are usually conducted within some fixed ranges of material properties, and in some cases we have to consider the boundary conditions, which is hardly reproduced in the tests. For obtaining widely applicable constitutive models, the experiments should consist of test specimens that systematically cover a wide range of geometrical as well as mechanical properties. Hence, analytical parametric study is preferred ahead of extensive experimental study, and some available experimental results are used to justify the analytical method and also to verify the proposed constitutive equations.

Simulation of Bare Bar Buckling

Fiber Technique for Finite Element Method Microanalysis

A three-dimensional nonlinear finite element program called COM3 [Concrete Model in 3D] (Tsuchiya et al. 1999) is used for the analytical parametric study. Nonlinear space frame elements analyzed by fiber technique (Menegotto and Pinto 1973) are used to model reinforcing bars. In fiber technique, each element is represented using a single line coinciding with the centerline of the member. The member cross section is divided into many cells or subelements. The strain of each cell is calculated based on the Euler-Kirchoff's hypothesis, i.e., plane section remains plane after bending. For each fiber strain along the axis of finite element, response is calculated using the material constitutive models representing the local behavior. The implementation of fiber technique is briefly illustrated in Fig. 1.

[1]Research Fellow, School of Civil and Structural Engineering, Nanyang Technological Univ., 50 Nanyang Ave., Singapore 639798; formerly, Graduate Student, Univ. of Tokyo. E-mail: cdhakal@ntu.edu.sg

[2]Professor, School of Civil Engineering, Univ. of Tokyo, Hongo 7-3-1, Bunkyo-Ku, Tokyo 113, Japan. E-mail: maekawa@concrete.t.u-tokyo.ac.jp

Note. Associate Editor: C. Dale Buckner. Discussion open until February 1, 2003. Separate discussions must be submitted for individual papers. To extend the closing date by one month, a written request must be filed with the ASCE Managing Editor. The manuscript for this paper was submitted for review and possible publication on April 28, 2000; approved on January 23, 2002. This paper is part of the ***Journal of Structural Engineering***, Vol. 128, No. 9, September 1, 2002. ©ASCE, ISSN 0733-9445/2002/9-1139–1147/$8.00+$.50 per page.

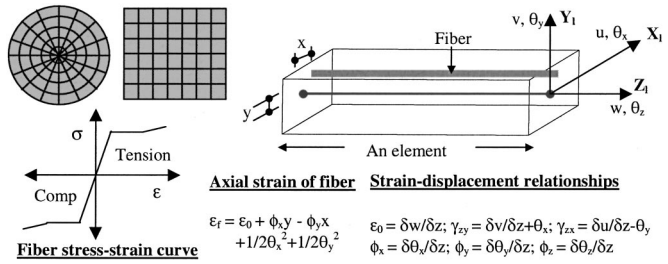

Fig. 1. Fiber technique adopted in finite element method micro-analysis

In this study, isoparametric elements with three nodes are used. In each node, six degrees of freedom are considered, i.e., the displacements (u, v, and w) and rotations (θ_x, θ_y, and θ_z) in three mutually perpendicular directions (local axes X_l, Y_l, and Z_l). Displacement field for an element is calculated from the nodal displacements and the assumed quadratic shape functions. Next, strain-displacement relationships are used to compute generalized strains, which include an axial component (ε_0), two shear components (γ_{zy}, γ_{zx}), and three curvatures (ϕ_x, ϕ_y, and ϕ_z). Based on these generalized strains, the average axial strain of each fiber ε_f is computed. Based on this axial strain, fiber axial stress is calculated from the point wise stress-strain relationship. These fiber stresses across the cross section are integrated to obtain the stress carried by the element.

The last two terms (second-order derivative terms) in the computation of average axial fiber strain includes the change in geometry due to large displacement of the reinforcing bars during loading. In small strain problems, where the geometry of the structure basically remains unchanged, these higher-order terms can be neglected. However, large lateral displacement of reinforcing bars cannot be captured without giving due consideration to geometrical nonlinearity. This fact is analytically proved afterwards.

Preliminary Microanalysis

The reinforcing bar is modeled as a vertical column of length L and diameter D. The total length L is discretized into several small elements. Monotonic downward displacement Δ is applied at the top of the reinforcement. To represent bare bar compression tests, the two ends of the reinforcing bars are represented by fixed nodes; i.e., both displacement and rotation are not allowed to take place. An elastic-perfectly plastic point wise stress-strain relationship with yield strength equal to 400 MPa and Young's modulus equal to 200 GPa is adopted.

First of all, a pair of analyses with and without considering geometrical nonlinearity is performed, and the average responses are compared in Fig. 2(a). If geometrical nonlinearity is not considered; i.e., the second-order terms are neglected in the computation of fiber strain, the postyield buckling phenomenon cannot be predicted, and the average response becomes the same as the point wise response. Next, mesh sensitivity analysis is conducted to obtain the influence of mesh discretization in average response. A reinforcing bar of length $L=16$ cm, diameter $D=16$ mm, and yield strength $f_y=400$ MPa is analyzed with varying number of elements. The average load-displacement curves are compared in Fig. 2(b). Using only one element to represent the bar rendered the average response similar to the assumed elastoplastic local behavior, and could not predict the softening of the average compression in spite of considering geometrical nonlinearity. As expected, the postbuckling average responses obtained using finer elements exhibit increased softening, and the mesh dependency nearly vanishes for more than four elements. Hence, at least four or more elements are used for further analyses.

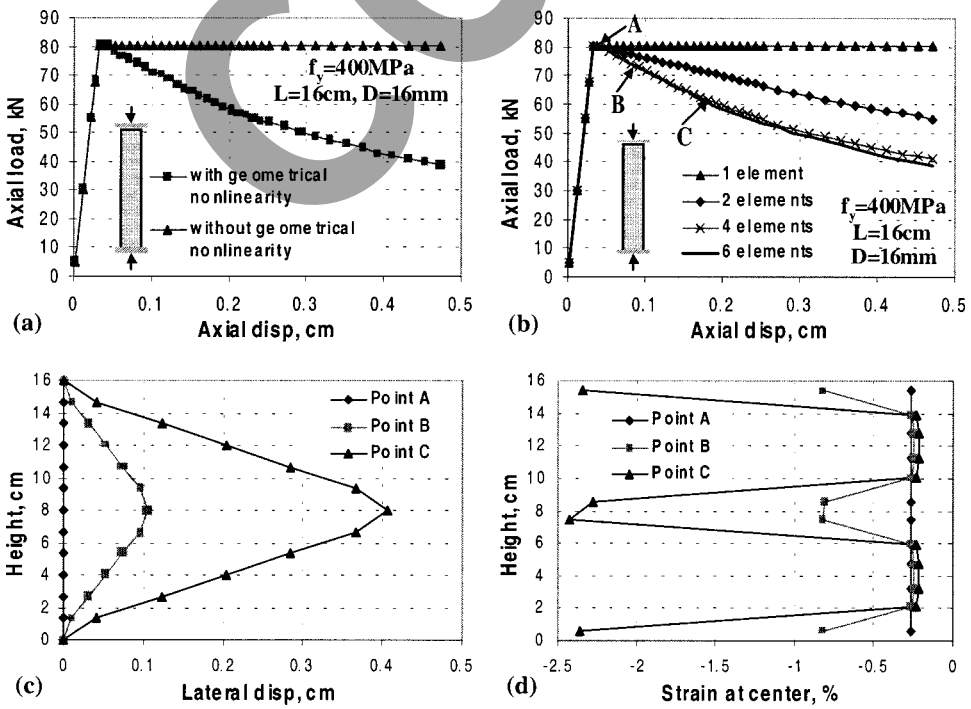

Fig. 2. (a) Effect of geometrical nonlinearity; (b) effect of mesh dicretization; (c) lateral displacement profile along length; and (d) variation of average strain along length.

J. Struct. Eng., 2002, 128(9): 1139-1147

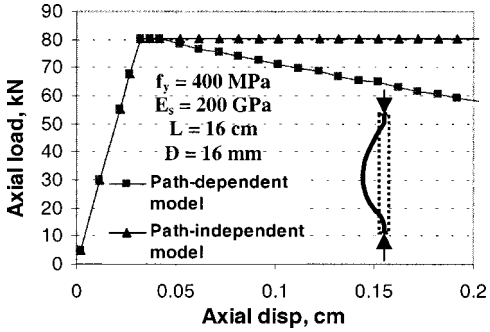

Fig. 3. Effect of path dependency on average response

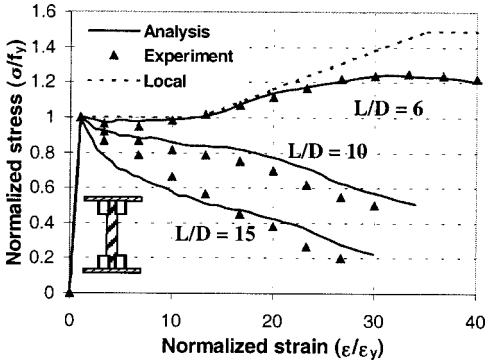

Fig. 4. Comparison with experimental results (Mander et al. 1984)

Next, the lateral deformation profile and distribution of fiber strain along the bar length are explained. Three instants denoted by points *A*, *B*, and *C* in Fig. 2(b) are selected for comparison. Point *A* refers to the instant just before the average stress starts decreasing, and points *B* and *C* lie in the softening phase. The lateral displacement profiles plotted in Fig. 2(c) indicate that the bar deforms laterally only after point *A*, and this lateral deformation is maximum at the midheight. Similarly, the average strain (strain at the center of the cross-section) profiles plotted in Fig. 2(d) reveal that the bar experiences uniform compression until point *A*, i.e., the starting point of buckling. This uniformity is lost afterwards and some portions, especially near the fixed support and around the midheight, experience continuous increase in compressive strain while strains in other parts decrease. Due to the curvature induced by lateral deformation, different fibers in the same cross section undergo hardening and unloading depending on the position of the fibers. The difference between hardening and unloading stiffness contributes to the decrease in the average stress.

General Discussion on Finite Element Method Microanalysis

In the mesh for microanalysis, all nodes of all elements were perfectly aligned along the same vertical line and no initial imperfection was provided to induce lateral deformation. In spite of this fact, the analytical solution could capture the buckling mechanism. The two possible modes of deformation of a bar under axial compression are axial mode representing longitudinal shortening and bending mode representing the usual buckling shape. The axial mode always leads to point wise stress-strain behavior whereas the bending mode triggers the softening of average stress provided that the material nonlinearity and path dependency are considered in the constitutive model. Both of these modes satisfy the requirements; i.e., the compatibility, equilibrium, and the constitutive equations. However, the energy associated with bending mode is smaller than that with axial mode. Hence, if geometrical nonlinearity is considered and the intermediate nodes are free to deform laterally, the finite element solution selects the bending mode, as it requires less energy during the nonlinear iteration process.

For further understanding, the analysis of a bar under compression was performed with geometrical nonlinearity but without any path dependency; i.e., stress reversal during cyclic loading was not considered. In other words, once the compressive strain exceeds yielding strain, the stress is kept constant regardless of the strain path (unloading or reloading). As shown in Fig. 3, the average stress-strain curve in this case is found to be the same as the point wise stress-strain relationship in spite of the presence of large lateral deformation. Although high curvature (strain gradient) across the section could be observed, the stresses at all fibers were equal because of the path-independent constitutive model. Consequently, in spite of geometrical nonlinearity, average compressive stress did not decrease.

Euler's theorem is commonly used to calculate the buckling load of axially compressed longitudinal bars. However, it is based on the assumption that the bar behaves elastically throughout the loading. Hence, for short bars, the buckling load predicted by Euler's formula is usually higher than the yield load. But, because of the elastoplastic nature of the reinforcing bars, the load cannot linearly increase in the postyield range, and Euler's theory is no longer applicable. In this case, the FEM microanalysis predicts that the buckling starts in the plastic region, where the axial stress is slightly higher than or equal to yield stress but the strain is substantially higher than the yielding strain. Needless to mention, for bars with higher-slenderness ratio, buckling starts in the elastic range, and Euler's formula gives a better prediction of buckling load, which is smaller than the yield load.

The softening of average compressive stress in postbuckling range is due mainly to the difference between the stiffness for postyield loading and unloading paths. The average response depends on both geometrical nonlinearity and the path dependency, and the influence of path dependency becomes crucial only when the geometrical nonlinearity is taken into account. On the other hand, the lateral deformation can be simulated only with geometrical nonlinearity but the softening of the postbuckling average stress cannot be captured without considering the path dependency in the nonlinear material model. The above discussions suggest that the average compressive behavior is not unique but depends on the mechanical properties of the reinforcing bars. However, if unloading and hardening properties are known in advance, the correct average constitutive model of reinforcing bars with any type of point wise stress-strain relationship can be analytically obtained.

Verification and Parametric Study

Verification of Microanalysis

For verification of the analytical method, the computed results are compared with experimental ones (Mander et al. 1984). The experiment consists of direct compression tests of five short medium-strength ($f_y = 290$ MPa, $E_s = 200$ GPa) reinforcing bars with different slenderness ratios (5.5, 6, 6.5, 10, and 15). The

J. Struct. Eng., 2002, 128(9): 1139-1147

normalized average compressive stress-strain curves are compared in Fig. 4. Note that the material model used in the verification analysis represents the result of sample bar test, which exhibits reasonable hardening [ε_{sh} (strain at hardening initiation)$=11.7\,\varepsilon_y$; E_{sh} (linear hardening stiffness)$=0.022\,E_s$; σ_n (maximum stress)$=433$ MPa]. The experimental and analytical curves are compared for only three different slenderness ratios, as the results corresponding to slenderness ratios 5.5, 6, and 6.5 are found to be very close to each other in experiment as well as analysis, and only one representative case ($L/D=6$) among these three was chosen. The results of FEM microanalysis are in good agreement with the experimental curves giving ample proof of the reliability of the analysis.

Next, the monotonic tests of Monti and Nuti (1992) are adopted for the verification of monotonic behavior. The experiment consists of a series of monotonic tests on steel reinforcing bars with different slenderness ratios (5, 8, and 11), and three different bar diameters of 16, 20, and 24 mm were used for each slenderness ratio. Here, the average of the three responses (with different diameters) for each slenderness ratio is used for comparison with FEM microanalysis. As the details of the material properties were not mentioned, the local behavior was fairly assumed to match the average response of the bar with slenderness ratio 5 because it was reported that the behavior of this shortest bar almost coincides with the local response. Hence, the following values were adopted: [$E_s=200$ GPa; $f_y=480$ MPa; ε_{sh} (strain at hardening initiation)$=2\,\varepsilon_y$; E_{sh} (linear hardening stiffness)$=0.055\,E_s$; σ_u (maximum stress)$=690$ MPa]. The comparative stress-strain curves are shown in Fig. 5. It can be observed that the results of FEM microanalysis are in fair agreement with the experimental results for all three cases of monotonic loading. However, a small difference can be observed in the early hardening range of the bar with slenderness ratio 5. This is due to the fact that the nonlinear hardening of the bar with slenderness ratio 5 was represented by using an average linear hardening range in the point wise stress-strain relationship. These verifications give ample evidence that the coupled geometrical and path-dependent material nonlinear analysis can reliably predict the buckling mechanism and also the average stress-strain behavior of axially compressed reinforcing bars.

Effect of Length and Diameter

It is well known that the average behavior of the reinforcing bar is very sensitive to its length and diameter. To elaborate more in this regard, two sets of parametric analyses are conducted with constant diameter and different lengths as well as constant length and different diameters. The normalized average responses are compared in Figs. 6(a and b). The softening of average stress becomes steeper with the increase in the reinforcement length provided that the bar diameter is constant. Similarly, if the reinforcement length is kept constant, the softening becomes milder with an increase in bar diameter. Both of these give similar qualitative relationship; i.e., the more slender the bar, the more severe the softening of average stress becomes. In order to obtain quantitative interrelationship, two pairs of cases, so that the slenderness ratio (length-to-diameter ratio) is the same but the length and diameter are different, are compared in Fig. 6(c). Irrespective of the different values of length and diameter, the normalized average response is similar for the same slenderness ratio. Finally, the normalized average responses for different slenderness ratios, assuming elastic-perfectly plastic behavior and $f_y=400$ MPa, are shown in Fig. 6(d). Agreeing with the conclusions of previous studies (Mau and El-Mabsout 1989; Monti and Nuti 1992; Dhakal and Maekawa 2000), it is found that the buckling is delayed and the degradation of postbuckling average stress is retarded with decrease in slenderness ratio of reinforcing bars.

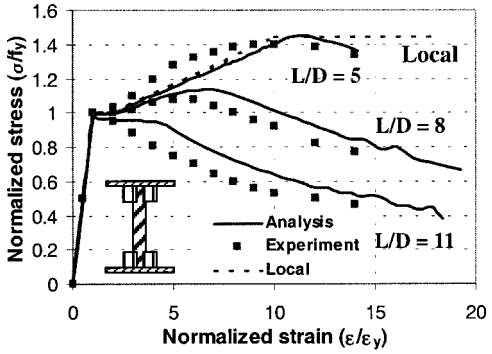

Fig. 5. Comparison with experimental results (Monti and Nuti 1992)

Effect of Yield Strength

The writers believe that the strength of the reinforcing bar also influences the average behavior in compression. To explore the inter-relationship, two sets of sensitivity analyses are performed with constant slenderness ratio and different yield strengths. The comparative normalized average stress-strain curves for slenderness ratios 5 and 10 and yield strengths ranging from 100 to 1,600 MPa are presented in Figs. 7(a and b), respectively. The softening of average stress becomes steeper with the increase in yield strength provided that the slenderness ratio is constant. Agreeing with previous study (Mau and El-Mabsout 1989), the average response of the high-strength bar is found to become more brittle than that of lower-strength bar. It was reported that the average response becomes nearly the same as the local response if L/D ratio is equal to or smaller than 5 (Mau 1990; Monti and Nuti 1992). However, the results suggested that this is not the reality, and this critical slenderness ratio depends on the yield strength of the reinforcing bar. For example, the average response of the bar with slenderness ratio 5 is very close to local response for $f_y=100$ MPa, but the difference between the local and average responses of a high-strength bar ($f_y=1{,}600$ MPa) with the same slenderness ratio is very big. Hence, rather than specifying the relationship in terms of slenderness ratio and yield strength separately, a combined term including both of these parameters seems more suitable.

For this purpose, two pairs of special cases [one pair each chosen from Figs. 7(a and b)] are compared with each other in Fig. 7(c). The first pair includes two cases, one with $f_y=100$ MPa; $L/D=10$ and the other with $f_y=400$ MPa; $L/D=5$. Similarly, the second pair includes cases with $f_y=400$ MPa; $L/D=10$ and $f_y=1{,}600$ MPa; $L/D=5$. The two cases in each pair were intentionally chosen to have equal value of $L/D\sqrt{f_y}$ in spite of different values for L/D and f_y. Interestingly, the normalized average responses of the two cases in each pair were exactly similar to each other, suggesting that there is a unique interrelationship between the parameter $L/D\sqrt{f_y}$ and the average response. Although some studies on modeling of average compressive response of reinforcing bars have been performed in the past (Mau and El-Mabsout 1989; Mau 1990; Monti and Nuti 1992), this unique interrelationship between yield strength and

J. Struct. Eng., 2002, 128(9): 1139-1147

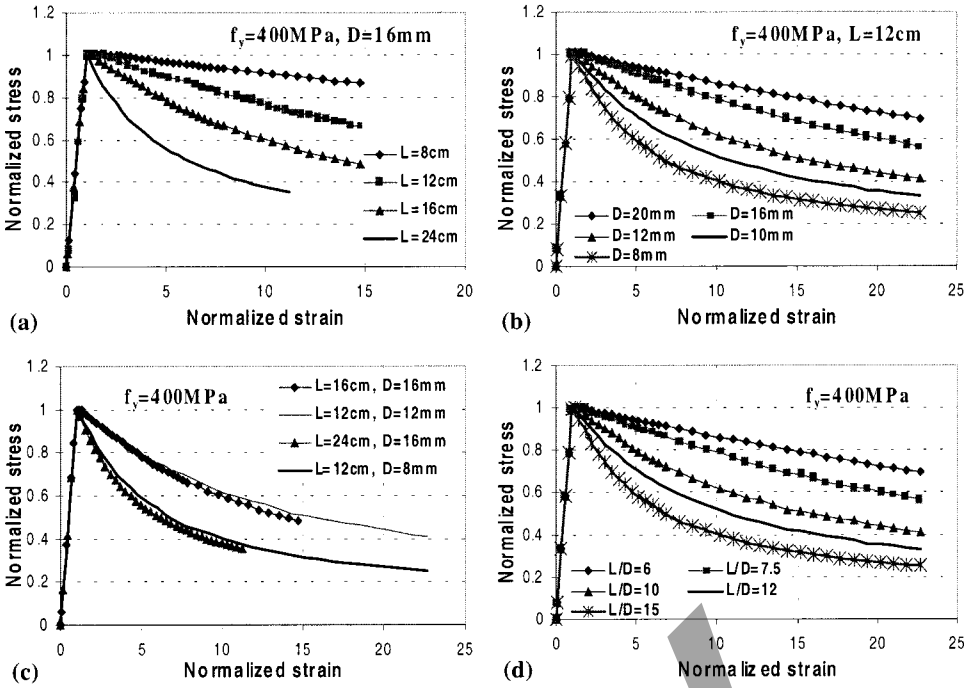

Fig. 6. Effect of length and diameter on average response

average compressive response was not realized. Next, the normalized average responses for different values of $L/D\sqrt{f_y}$, using elastic-perfectly plastic point wise stress-strain relationship, are shown in Fig. 7(d). As expected, buckling happens earlier and the postbuckling average stress degrades faster with an increase in the value of this parameter.

Reinforcing Bars with Strain Hardening

The earlier discussions were based on the microanalysis of reinforcing bars of elastic-perfectly plastic material. In contrast, commonly used reinforcing bars exhibit hardening after a yield plateau in the postyield range, though the hardening stiffness and

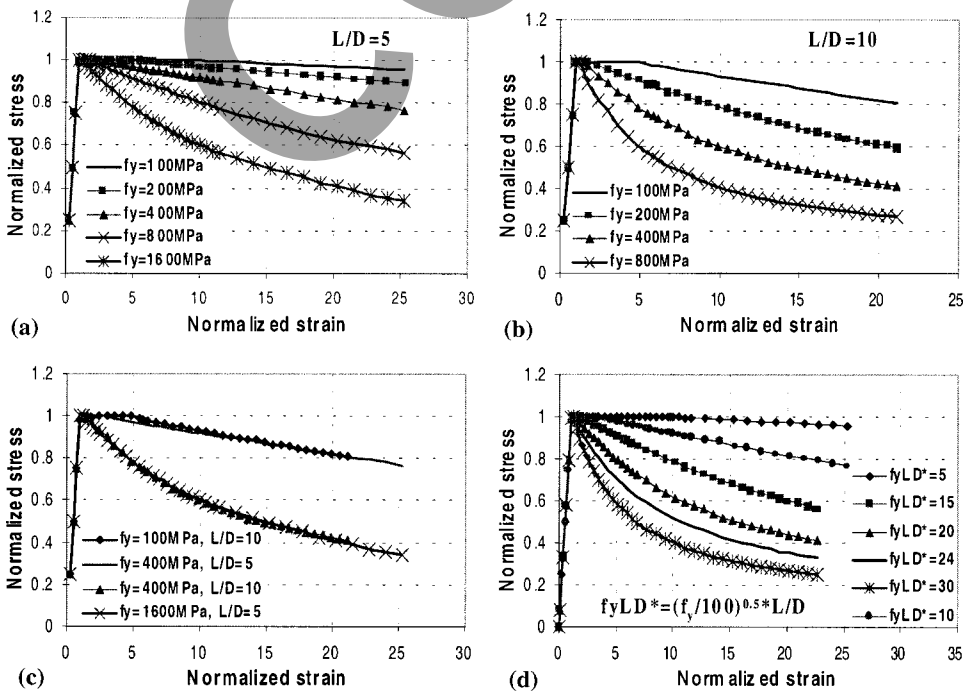

Fig. 7. Effect of yield strength on average response

J. Struct. Eng., 2002, 128(9): 1139-1147

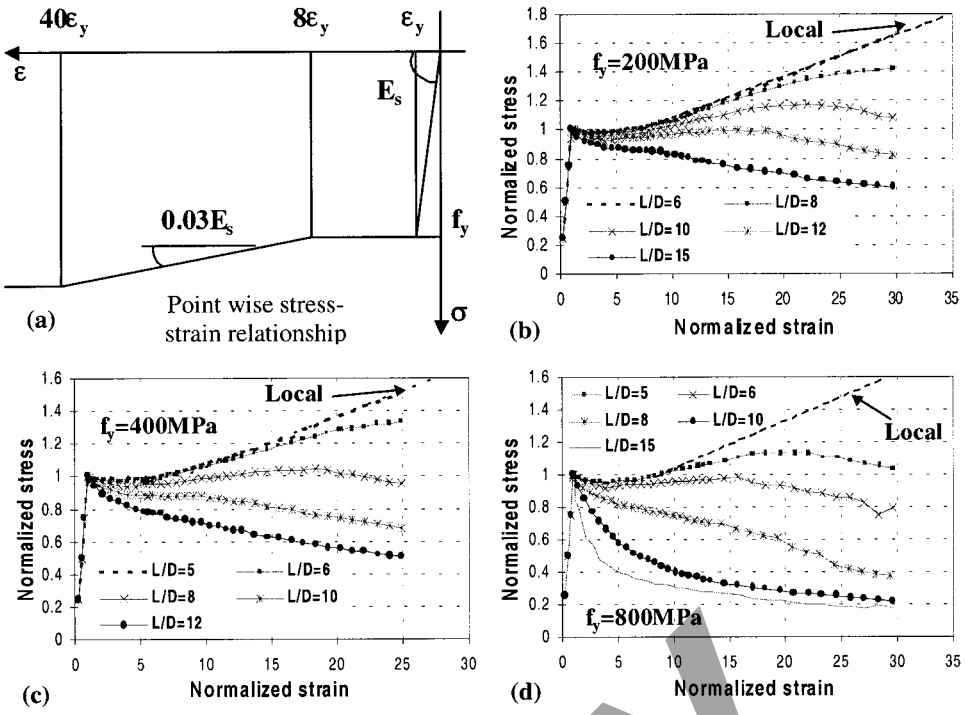

Fig. 8. Average responses of reinforcing bars with hardening

range may vary between the bars produced in different countries. To cover all types of reinforcing bars, the parametric study hereafter is conducted for linear hardening material, which along with elastic-perfectly plastic material constitute the two opposite extremes of all possible hardening mechanisms. The assumed point wise stress-strain relationship is shown in Fig. 8(a), and the average compressive stress-strain curves of bars with slenderness ratio varying between 5 and 15 are shown in Figs. 8(b–d) for yield strength equal to 200, 400, and 800 MPa, respectively. As expected, the softening of average postbuckling compressive stress for the same slenderness ratio becomes steeper with the increase in yield strength. Moreover, the starting point of negative slope is delayed, and the absolute value of normalized stress is also higher than that in elastoplastic bar.

Note that the negative slope of the average stress-strain curves in the later descending stage is nearly constant (approximately equal to 2% of Young's modulus), irrespective of the value of the parameter $L/D\sqrt{f_y}$. Similarly, the average compressive stress nearly becomes constant after it decreases to 20% of the yield strength. These behaviors were also seen in elastoplastic bars, and can greatly assist in the modeling of average compressive behavior of reinforcing bars. As in elastoplastic bars, the average response of these linear hardening bars also uniquely depends on the parameter $L/D\sqrt{f_y}$, irrespective of separate values of L, D, and f_y. As the responses of bars with these two extreme models (elastic-perfectly plastic and linear hardening) indicate similar inter-relationships between the slenderness ratio, yield strength, and the average compressive response, the same should be applicable to reinforcing bars with any hardening mechanisms. Hence, the limiting L/D ratio below which the average behavior is close to the material model can be better approximated by a multiple of $(1/\sqrt{f_y})$ rather than a constant value regardless of bar strength as recommended in previous studies.

Average Stress-Strain Relationship

Through the analytical parametric study, various facts regarding the average behavior of reinforcing bars in compression are revealed. Some of them are: (1) the average compressive stress-strain relationship depends only on the product of slenderness ratio and the square root of yield strength; (2) the average compressive stress becomes smaller than the point wise stress after the initiation of buckling, and the starting point of average stress degradation also depends on the point wise stress-strain relationship; (3) the stress degradation rate in the later stage of postbuckling average stress-strain curve is nearly constant with a negative slope approximately equal to 2% of the Young's modulus; and (4) the average post-buckling compressive stress becomes constant after it decreases to 20% of the yield strength.

Guided by these unique inter-relationships, an average monotonic compressive stress-strain model is proposed, the general layout of which is sketched in Fig. 9. An intermediate point (ε^*,σ^*) is established, after which a constant negative stiffness equal to $0.02E_s$ is assumed until the average stress becomes equal to $0.2f_y$. To represent the aforementioned mechanisms, the fol-

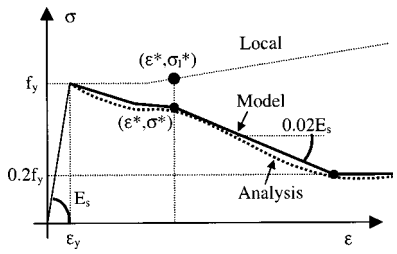

Fig. 9. Schematic representation of proposed model

J. Struct. Eng., 2002, 128(9): 1139-1147

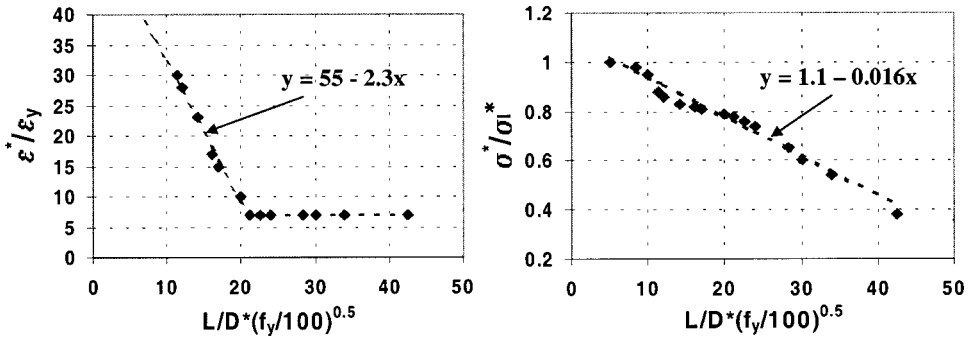

Fig. 10. Determination of coordinates of intermediate point

lowing equations relating the average compressive stress with the average compressive strain of reinforcing bar are proposed:

$$\frac{\sigma}{\sigma_l}=1-\left(1-\frac{\sigma^*}{\sigma_l^*}\right)\left(\frac{\varepsilon-\varepsilon_y}{\varepsilon^*-\varepsilon_y}\right);\quad \text{for } \varepsilon_y<\varepsilon\leqslant\varepsilon^*$$
$$\sigma\geqslant 0.2f_y;\quad \sigma=\sigma^*-0.02E_s(\varepsilon-\varepsilon^*);\quad \text{for } \varepsilon>\varepsilon^* \tag{1}$$

Here, σ_l and σ_l^*=point wise stresses corresponding to ε (current strain) and ε^* (strain at intermediate point), respectively. Similarly, ε_y and E_s=yielding strain and Young's modulus of the reinforcing bar. To make the model applicable to bars with all types of material model, the stresses at and before the intermediate point are normalized with respect to the stresses computed from the point wise stress-strain relationship at the corresponding strain value. This normalization technique also allows for the shape of the average response before this intermediate point to look like point wise stress-strain curve, a behavior which was distinctly observed in all microanalysis results. The coordinates of the intermediate point (ε^*,σ^*) can be calculated by means of the following equations:

$$\frac{\varepsilon^*}{\varepsilon_y}=55-2.3\sqrt{\frac{f_y}{100}}\frac{L}{D};\quad \varepsilon^*/\varepsilon_y\geqslant 7 \tag{2}$$

$$\frac{\sigma^*}{\sigma_l^*}=\alpha\left(1.1-0.016\sqrt{\frac{f_y}{100}}\frac{L}{D}\right);\quad \sigma^*\geqslant 0.2f_y \tag{3}$$

Note that Eqs. (2) and (3) are derived from the microanalysis results of bars with linear hardening behavior plotted in Fig. 10. When checked with the results of elastic-perfectly plastic bars, it was found that the normalized strain at the intermediate point ε^* was not much different, and Eq. (2) was still applicable without any amendment. Nevertheless, the normalized value of stress at the intermediate point σ^* was smaller than that in linear hardening bars. Hence, for bars with more realistic hardening model, $\varepsilon^*/\varepsilon_y$ is expected to be unaffected but σ^*/σ_l is expected to be smaller than in linear hardening bars and larger than in elastoplastic bars. To account for this change, a coefficient α is included in the formulation of σ^*. For the two extreme cases assumed earlier for the parametric study, the value of α is found to be 1.0 for linear hardening bars, and 0.75 for perfectly elastoplastic bars.

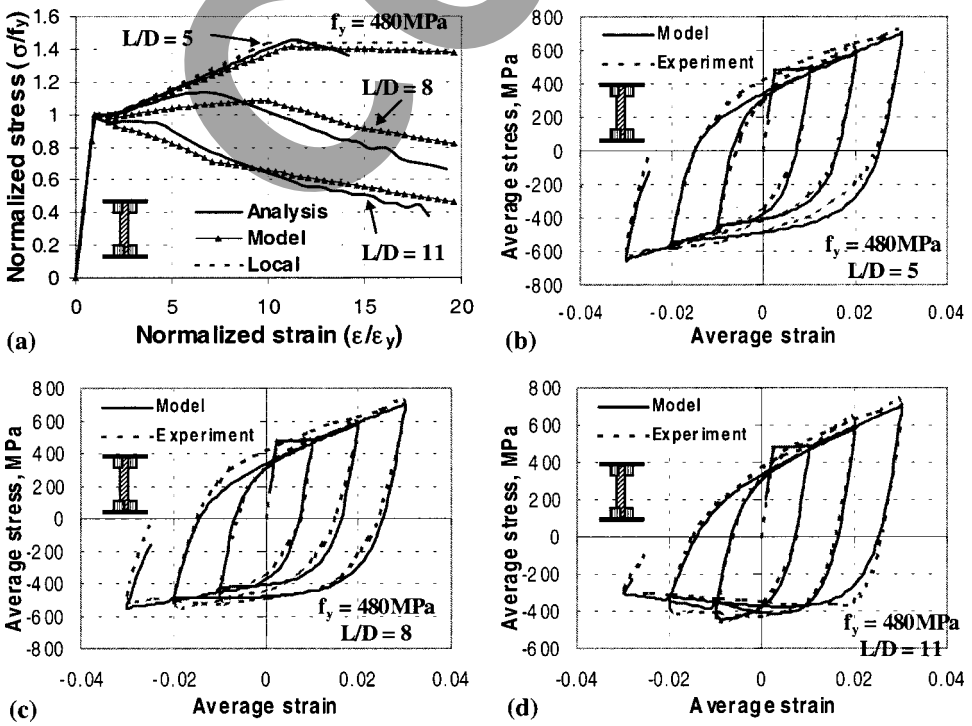

Fig. 11. Comparison with monotonic and cyclic test results (Monti and Nuti 1992)

J. Struct. Eng., 2002, 128(9): 1139-1147

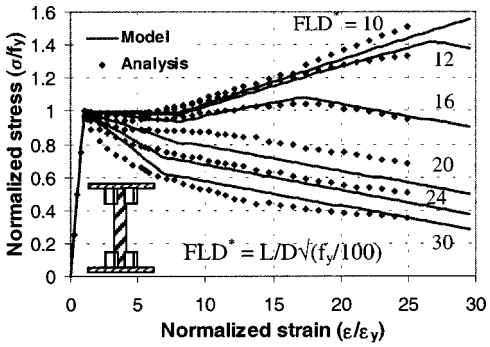

Fig. 12. Comparison of model with microanalysis (continuous linear hardening)

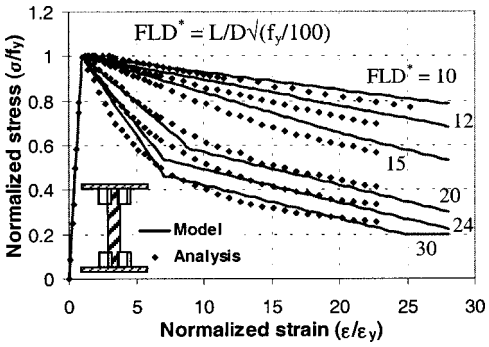

Fig. 13. Comparison of model with microanalysis (elastic-perfectly plastic)

For bars with limited hardening range, in which most of the industrial products fall, it should be chosen between 0.75 and 1. If the hardening stiffness is very small and the hardening range in terms of strain is short, the value should be closer to 0.75. In contrast, if the hardening stiffness is significant and lasts for large strain range, α should be closer to 1.0.

As the framework for unloading and reloading behavior in strain reversal, the authors adopt the Giuffre-Menegotto-Pinto model (CEB 1996) assuming reduced reloading stiffness from postbuckling compression state, as observed in experiments (Monti and Nuti 1992; Suda et al. 1996). To control the smoothness of the transition curves, the cyclic model uses a parameter R computed from three constants R_0, a_1, and a_2 to be determined experimentally. Provided that the resulting value of R is positive, the transition becomes smoother if the value of a_1 increases or that of R_0 and a_2 decreases. As these constants do not influence the monotonic curve and small changes in their values marginally affect the transition shapes during strain reversals, the authors have adopted $R_0=20$; $a_1=18.5$; and $a_2=0.15$ after extensive checking. A complete path-dependent cyclic model relating the average stress with average strain can now be formulated by combining the proposed monotonic compressive average stress-strain relationship with tension envelope of the bare bar and the Giuffre-Menegotto-Pinto model for the unloading/reloading loops.

Verification of Proposed Computational Model

First, the performance of the proposed model is compared with FEM microanalysis and experimental results of the monotonic tests (Monti and Nuti 1992) in Fig. 11(a) As the point wise cyclic stress-strain relationship of the bar material was not reported, the FEM microanalysis could not be carried out for cyclic tests, and the average cyclic responses observed in the experiment are compared only with those computed by the proposed model, as illustrated in Figs. 11(b–d) for slenderness ratios 5, 8, and 11, respectively. As the hardening stiffness in the material model is significant ($0.055E_s$) but lasts only for $8\varepsilon_y$, the coefficient in the proposed model is assumed as $\alpha=0.9$ according to the earlier recommendation. As seen in the figure, the monotonic curves predicted by the model for different slenderness ratios are close to the FEM microanalysis and experimental results. Moreover, it can also be observed that the proposed model is in good agreement with the experimental results for all three cases of cyclic loading, giving ample evidence that the proposed monotonic average compressive stress-strain relationship combined with Giuffre-Menegotto-Pinto cyclic model can be reliably used.

Nevertheless, the verification for cyclic loading is conducted within the range of 3% tensile and compressive strains; i.e., around 15 times yield strain for normal strength bars. Although 3% compressive strain is difficult to be reached, larger tensile strain can be induced in reinforcing bars inside RC structures during strong earthquakes. Test data measuring much higher strain are scarce, which might be due to the difficulty in measuring higher strain with the commonly used strain gauges. Note that the average compressive stress of the most slender bar ($L/D=11$) unloaded from large tensile strain starts to decrease before reaching the compressive strain zone because of the negative slope at the target point. This behavior is qualitatively supporting the outcome of previous study (Rodriguez et al. 1999) that the compressive stress degradation point (termed as buckling onset point) depends on the maximum tensile strain reached before a strain reversal. The effect of maximum tensile strain might be more pronounced if the strain reversal is from much larger strain, and the proposed model needs to be verified for such large strain cyclic tests before drawing quantitative conclusions.

Next, the proposed model is compared with FEM microanalysis for two extreme cases. Figs. 12 and 13 show the comparison between the proposed model and FEM analysis for reinforcing bars with continuous linear hardening and elastic-perfectly plastic material models, respectively. The comparisons are performed for different values of the parameter $FLD^*=L/D\sqrt{(f_y/100)}$. As established earlier, the coefficient α in the proposed model is assumed as unity for the linear strain hardening case and 0.75 in elastic-perfectly plastic case. Average responses predicted by the proposed model are very close to those by FEM microanalysis for almost all cases. As the model is valid for these two extreme cases, the authors believe that it can represent the behavior of bars with any hardening range. The earlier verification of the models with the test data of bars with reasonable hardening range also advocates this claim.

Conclusions

Microanalyses based on fiber technique using finite elements with small size were conducted to predict the average behavior of reinforcing bars in compression accompanying geometrically large nonlinearity. It was revealed that the average compressive behavior depends only on one parameter; i.e., $L/D\sqrt{f_y}$ (product of slenderness ratio and square root of yield strength). It was also found that the conclusion from some previous studies, stating that the average compressive response of reinforcing bars with slenderness ratio equal to or less than 5 is the same as the local response,

J. Struct. Eng., 2002, 128(9): 1139-1147

is not always true, especially in the case of high-strength bars. Based on the results of the parametric study, an average compressive stress-strain model is proposed that can be applied for reinforcing bars with any geometrical as well as mechanical properties. Giuffre-Menegotto-Pinto model for cyclic loops is combined with the proposed model to yield a complete path-dependent cyclic model. The comparison of the microanalysis as well as the proposed model with some experimental results showed good agreement and verified the reliability of proposed model for both monotonic and cyclic loading.

Acknowledgments

The writers gratefully acknowledge TEPCO Research Foundation and Grant-in-aid for scientific research No. 11355021 for providing financial support to accomplish this research.

Notation

The following symbols are used in this paper:

D = diameter of reinforcing bar;
E_s = Young's modulus of reinforcing bar;
E_{sh} = hardening stiffness;
f_y = yield strength of reinforcing bar;
L = test length of reinforcing bar;
α = coefficient depending on local behavior of bar;
ε, σ = average strain and average stress;
ε^*, σ^* = strain and stress at intermediate point;
ε_{sh} = strain at hardening initiation point;
ε_y = yield strain of reinforcing bar;
σ_u = maximum stress carried by reinforcing bar; and
σ_l, σ_l^* = local stresses at current strain and ε^*, respectively.

References

Comité Euro-International du Béton (CEB) (1996). *RC elements under cyclic loading—State-of-the-art report*, Thomas Telford, Paris.

Dhakal, R. P., and Maekawa, K. (2000). ''Postpeak cyclic behavior and ductility of reinforced concrete columns.'' *Modeling of inelastic behavior of RC structures under seismic loads*, ASCE, New York, 193–216.

Dodd, L. L., and Restrepo-Posada, J. I. (1995). ''Model for predicting cyclic behavior of reinforcing steel.'' *J. Struct. Eng.*, 121(3), 433–445.

Mander, J. B., Priestley, M. J. N., and Park, R. (1984). ''Seismic design of bridge piers.'' *Research Rep. No. 84-2*, Dept. of Civil Engineering, Univ. of Canterbury, New Zealand.

Mau, S. T. (1990). ''Effect of tie spacing on inelastic buckling of reinforcing bars.'' *ACI Struct. J.*, 87(6), 671–678.

Mau, S. T., and El-Mabsout, M. (1989). ''Inelastic buckling of reinforcing bars.'' *J. Eng. Mech.*, 115(1), 1–17.

Menegotto, M., and Pinto, P. E. (1973). ''Method of analysis of cyclically loaded RC plane frames including changes in geometry and nonelastic behavior of elements under normal force and bending.'' *Preliminary Rep. IABSE*, Zurich, 13, 15–22.

Monti, G., and Nuti, C. (1992). ''Nonlinear cyclic behavior of reinforcing bars including buckling.'' *J. Struct. Eng.*, 118(12), 3268–3284.

Rodriguez, M. E., Botero, J. C., and Villa, J. (1999). ''Cyclic stress-strain behavior of reinforcing steel including the effect of buckling.'' *J. Struct. Eng.*, 125(6), 605–612.

Suda, K., Murayama, Y., Ichinomiya, T., and Shimbo, H. (1996). ''Buckling behavior of longitudinal reinforcing bars in concrete column subjected to reverse lateral loading.'' *Proc., 11th World Conf. on Earthquake Engineering*, CD ROM Paper No. 1753, Acapulco, Mexico.

Tsuchiya, S., Ogasawara, M., Tsuno, K., Ichikawa, H., and Maekawa, K. (1999). ''Multiaxial flexura behavior and nonlinear analysis of RC columns subjected to eccentric axial forces.'' *J. Mater., Concr. Struct. Pavements, JSCE*, 634(45), 131–144.